DOI: 10.1002/ejic.200900335

Syntheses and Characterization of Lead(II) *N*,*N*-Bis[1(2)*H*-tetrazol-5-yl]amine Compounds and Effects on Thermal Decomposition of Ammonium Perchlorate

Weitao Wang,[a] Sanping Chen,[a] and Shengli Gao*[a]

Keywords: Lead / Nitrogen heterocycles / Perchlorates / Luminescence

Three new lead(II) *N*,*N*-bis[1(2)*H*-tetrazol-5-yl]amine (H_2bta) compounds, $[Pb(bta)(H_2O)_2]_n$ (**1**), $[Pb_2(bta)_2(bpy)_2]$ (**2**), and $[Pb_2(bta)_2(phen)_2]\cdot 2H_2O$ (**3**), were synthesized. Single-crystal X-ray diffraction reveals that compound **1** has a 1D polymeric zigzag chain structure, whereas compounds **2** and **3** have binuclear structures. In addition, compounds **1**–**3** were explored as additives to promote the thermal decomposition of ammonium perchlorate by differential scanning calorimetry. (© Wiley-VCH Verlag GmbH & Co. KGaA, 69451 Weinheim, Germany, 2009)

Introduction

Research in the field of highly energetic materials is nowadays directed towards the synthesis of simple molecules with high energy, high density, high heat resistance, and low sensitivity.[1] Nitrogen-rich compounds rely on their highly efficient gas production and high heat of formation for energy release, as elemental nitrogen, which has a zero heat of formation, is the major product of decomposition.[2] Tetrazole possesses an unsaturated five-membered heterocycle with four nitrogen atoms in the ring. The high nitrogen content of tetrazole and its derivatives allows these compounds to serve as potential energetic materials. *N*,*N*-bis[1(2)*H*-tetrazol-5-yl]amine (H_2bta), also known as bis(tetrazolyl)amine, has been studied due to its versatile coordinate mode for building microporous metal–organic frameworks, interesting network topologies, and potential application as molecular magnets.[3–8] It is predicted that salts of bta exhibit the potential application as additives in pyrotechnics and propellants.[9–11] However, salts of bta as additives in propellants are rarely reported.

Ammonium perchlorate (AP) is the common oxidizer in composite solid propellants, and the thermal decomposition characteristics of AP directly influence the combustion behavior of solid propellants.[12,13] Many effective combustion catalysts on the thermal decomposition of AP, such as metal oxides, which are not nitrogen-rich or energetic compounds, have been reported.[14–20] We anticipate salts of bta would work as 3-nitro-1,2,4-triazol-5-one (NTO) compounds,[21,22] which affect the thermolysis of AP.

In order to study the effects of bta salts on the thermal decomposition of AP, we choose metal lead(II) on the basis of the following considerations: (1) Lead(II) shows good catalytic performances for propellants.[23] (2) Lead(II), as a result of the stereochemical activity of the lone electron pair, possesses a large radius, a variable stereochemical activity, and a flexible coordination mode.[24–26] (3) Lead(II) compounds with bta remain unexplored although extensive studies on bta compounds have been reported. In this paper, we report the syntheses and structures of three coordination compounds with lead(II): $[Pb(bta)(H_2O)_2]_n$ (**1**), $[Pb_2(bta)_2(bpy)_2]$ (**2**), and $[Pb_2(bta)_2(phen)_2]\cdot 2H_2O$ (**3**) (bpy = 2,2′-bipyridine, phen = 1,10-phenanthroline). Furthermore, thermal gravimetric analysis, photoluminescent properties, and the catalytic performances toward thermal decomposition of AP are explored.

Results and Discussion

Structure of $[Pb(bta)(H_2O)_2]_n$ (1)

Singe-crystal X-ray diffraction reveals that the structure of **1** consists of 1D polymeric zigzag chains spanning two different directions perpendicular to the (101) plane, which, however, display a quite fascinating supramolecular organization. As shown in Figure 1, $[Pb(H_2O)_2]^{2+}$ units are joined by bta^{2-} spacers to generate a 1D zigzag chain with a period of 7.263 Å. Each Pb^{II} ion is coordinated by three nitrogen atoms from two bta^{2-} ligands and two oxygen atoms from water molecules, showing a square-pyramidal geometry. The basal plane is formed by atoms N4^{i}, N6, O1, and O2, with Pb1–N4^{i} 2.640(6) Å, Pb1–N6 2.527(6) Å, Pb1–O1 2.583(6) Å, and Pb1–O2 2.682(6) Å (i: 1/2 + *x*, 3/2 –*y*, 1/2 + *z*). The left apical position is occupied by N1 with Pb1–N1 2.461(6) Å. As a result of the stereochemically active lone pair, two secondary bonds, Pb1···O1^{ii} 2.863(6) Å,

[a] Key Laboratory of Synthetic and Natural Functional Molecule Chemistry of Ministry of Education, College of Chemistry and Materials Science, Northwest University,
Xi'an 710069, P. R. China
E-mail: gaoshli@nwu.edu.cn

Supporting information for this article is available on the WWW under http://dx.doi.org/10.1002/ejic.200900335.

Pb1···N3^{iii} 3.063(7) Å (ii: $-x$, 2 $-y$, 2 $-z$, iii: 1/2 $-x$, 1/2 + y, 3/2 $-z$), produce that the coordination number (CN) is seven with (5+E)+2.[24]

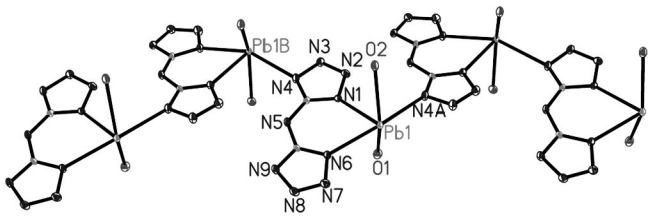

Figure 1. The zigzag chain of **1** (thermal ellipsoids: 30%, H atoms are omitted for clarity).

If a limit of 2.90 Å is placed upon Pb^{II}–O_w, **1** is a binuclear polymer with Pb···Pb 4.503 Å. It thus results in a 2D layer (Figure 2a) by bridging water O1, which is rarely reported for lead(II) compounds with tetrazole ligands.[27] Furthermore, the Pb···N weak interaction and hydrogen bonds (Table S2) expand the layer to be a 3D polymeric network, as shown in the Figure 2b.

(a)

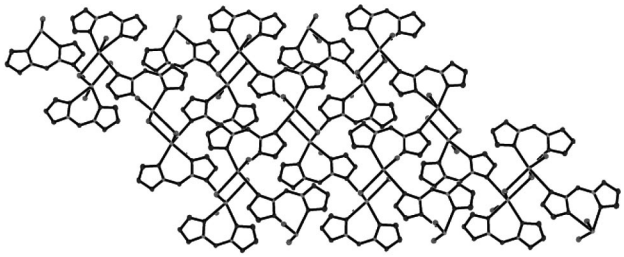

(b)

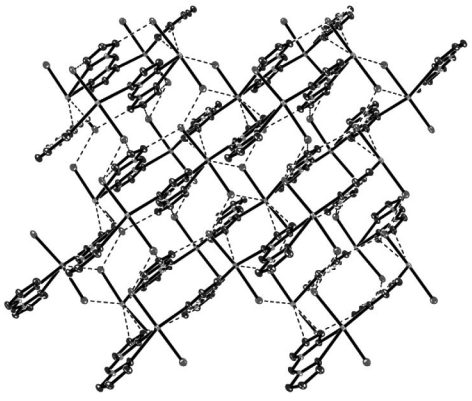

Figure 2. (a) 2D sheet viewed along the *a* axis; (b) 3D pack structure viewed along the *b* axis (H atoms are omitted for clarity).

Structure of $[Pb_2(bta)_2(bpy)_2]$ (2)

As shown in the Figure 3, **2** consists of neutral dimeric Pb(bta)(bpy) moieties. Each Pb^{2+} is linked to another inversion-related Pb^{2+} to give rise to a centrosymmetric dimeric unit, which can be described as a planar Pb2N4 six-mem-

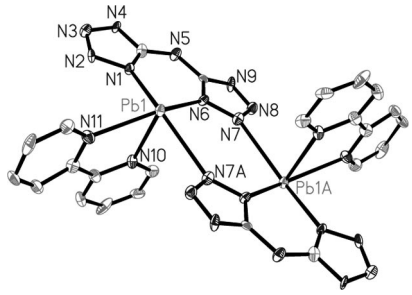

Figure 3. Coordination environment of Pb^{2+} in **2** (thermal ellipsoids: 30%, H atoms are omitted for clarity).

(a)

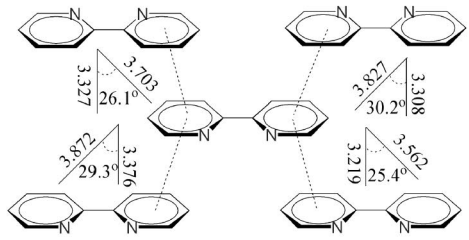

(b)

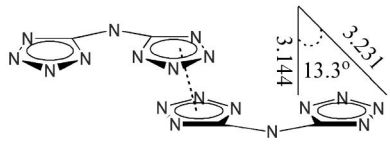

(c)

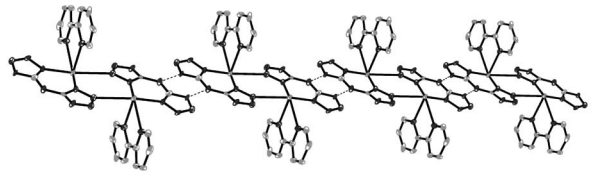

(d)

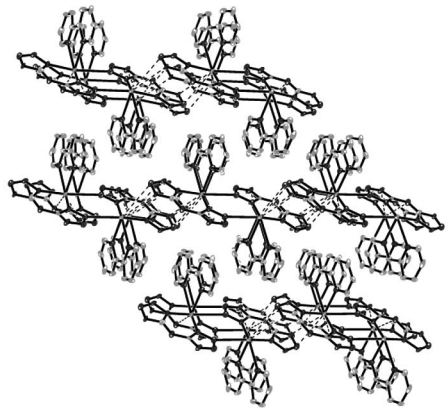

Figure 4. π–π stacking interactions of (a) the pyridine rings in the bpy ligands and (b) the tetrazole rings in the bta^{2-} ligand; (c) the 1D chain afforded by hydrogen bonds; (d) the 3D frame of **2** viewed along the *a* axis (H atoms are omitted for clarity).

bered ring; the Pb···Pb intramolecular separation (5.224 Å) is longer than that of binuclear polymer **1**. Each Pb^{2+} is coordinated by three N atoms from two bta^{2-} and two N atoms from bpy with Pb–N distances varying from 2.461(12) to 2.586(17) Å except the bridging bond Pb1···N7^{i} 2.791(15) Å (i: 2 – *x*, 1 – *y*, 1 – *z*), which is longer than the bridging N in **1**. The coordination polyhedron can be viewed as a square-pyramidal geometry. Additionally, three Pb···N weak interactions [Pb1···N3^{i} 3.408(17) Å, Pb1···N4^{i} 3.286(14) Å, Pb1···N9^{ii} 3.568(15) Å, i: 2 – *x*, 1 – *y*, –z; ii: –1 + x, *y*, *z*] give the coordination number of eight with (5+E)+3.[24]

Two pyridine rings in the bpy moiety are almost perpendicular to the Pb2N4 ring planar, with dihedral angles of 86.84 and 78.40°, respectively. Furthermore, every adjacent pyridine ring is involved in off-set face-to-face π–π interactions with centroid-to-centroid separations varying from 3.562 to 3.827 Å (Figure 4a). In addition, the neighbor tetrazole rings in bta^{2-} exhibit strong π–π stacking interactions with center-to-center distances of 3.291 Å (Figure 4b), which is less documented. The strong hydrogen bond ring motif [N5···N4^{iii} = 2.98(2) Å, iii: 3 – *x*, 1 – *y*, –*z*] is identified as the very common $R_2^2(8)$,[28] which bridge the dimeric units to the 1D chain (Figure 4c), where the Pb2N4 ring planes are parallel. Chains further expand into a 3D construction (Figure 4d) by π–π stacking interactions.

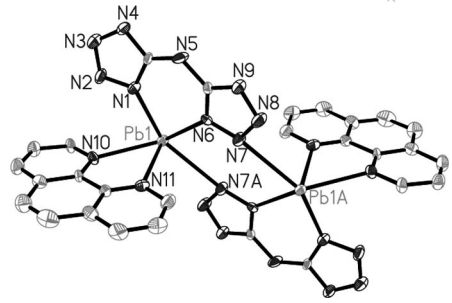

Figure 5. Coordination environment of Pb^{2+} in **3** (thermal ellipsoids: 30%, lattice water and H atoms are omitted for clarity).

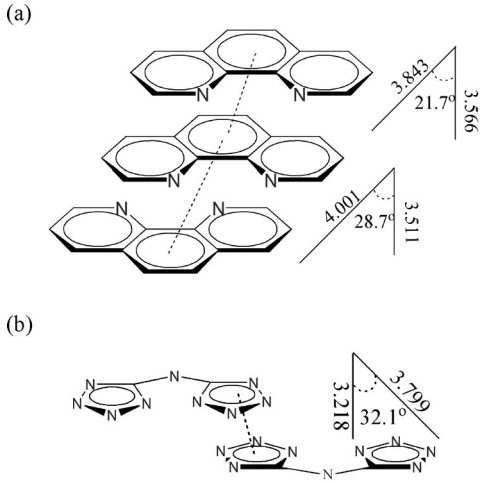

Figure 6. π–π stacking interactions of (a) the phen molecules and (b) the tetrazole rings in the bta^{2-} ligands; (c) the 1D chain afforded by hydrogen bonds in **3** (H atoms are omitted for clarity).

Structure of $[Pb_2(bta)_2(phen)_2]\cdot 2H_2O$ (3)

Although **2** and **3** crystallize in two different space groups, their units are very similar except that bpy is replaced by phen (Figure 5) and lattice water molecules are involved in **3**. For **3**, Pb^{2+} is coordinated in a square-pyramidal geometry with two weak interactions [Pb1···N4^{i} 3.167(13), Pb1···N8^{ii} 3.312(12), i: –*x*, –*y*, –*z*; ii: *x*, –*y*, 1/2 + *z*], leading to the coordination number of seven with (5+E)+2.[24] The Pb–N distances vary from 2.442(10) to 2.632(11) Å with exclusion of the bridging bond Pb1···N7^{iii} 2.848(12) Å (iii: 1 – *x*, –*y*, –*z*), which is longer than those in **1** and **2**. Two coplanar phen molecules (dihedral angle: 0.66°) in **2** are almost vertical to the Pb2N4 ring with dihedral angles of 77.26 and 76.60°, respectively. The Pb···Pb separation of the binuclear unit in **3** is 5.518 Å, which is longer than those in **1** and **2**. The centroid-to-centroid separations of the adjacent phen segments are 4.220 and 3.323 Å, alternatively, indicating significant π–π stacking effects (Figure 6a). Additionally, π–π interactions of the tetrazole rings (centroid-to-centroid: 3.799 Å; Figure 6b) are weaker than those in **2**. Compared with **2**, the dihedral angle of the Pb2N4 ring planes of the chains (Figure 6c) afforded by N5···N9^{i} (i:–*x*, *y*, –*z* – 1/2) in **3** is 44.5°, which may be due to the different π–π recognitions. The strong hydrogen bonds (Table S2) and π–π interactions extend the dimeric units to a supramolecule (Figure S1).

The dihedral angles of the two tetrazole rings in bta^{2-} (2.25° in **1**, 9.96° in **2** and 10.56° in **3**) and the separations of Pb···Pb increase. The two tetrazole rings in each bta^{2-} in **1** is nearly coplanar, as reported in the $Mn_3(Hbta)_4(\mu_2\text{-}OH)_2(H_2O)\cdot 2H_2O$[8] (4.23°) while the dihedral angle are almost equal in **2** and **3**, which may be attributed to the stereochemical activity of the lone pair electrons and coordination mode. The amino nitrogen of bta^{2-} ligand is involved in intramolecular hydrogen bonds in **1** and common $R_2^2(8)$ hydrogen bonds motif in both **2** and **3**. These indicate that the amino nitrogen in bta^{2-} is a good candidate for establishing hydrogen bonds supramolecule[3,29] (Figure 4c, Figure 6c). In addition, the tetrazole rings in the bta^{2-} ligand exhibit good π-π interactions[30] (Figure 4b, Figure 6b).

Thermal Gravimetric Analyses

Thermal gravimetric (TG) analysis was carried out between 30 and 900 °C (see Figures S2–S4 for TGA curves). In the TGA curve of **1**, the first weight loss of 9.41% in the range 160–290 °C corresponds to the expulsion of two coordinated water molecules (calcd. 9.13%). The remaining substance is unstable and a series of weight losses occur, which do not end until 655 °C. Compound **2** does not experience weight loss before 167 °C and then experiences consecutive steps with a mass loss of 74.53% (calcd. 69.11%),[10] which do not stop until 674 °C, corresponding to the losses of bta and bpy. Compound **3** remains stable up to 100 °C and then undergoes one-step weight loss of 6.31% from 100 to 270 °C, corresponding to the loss of the lattice water molecules (calcd. 5.01%), after that a series of weight losses up to 800 °C were observed.

Effects on Thermal Decomposition of Ammonium Perchlorate

Compounds **1**–**3** and AP were mixed at a mass ratio of 1:3 to prepare the target samples for thermal decomposition analyses. A total sample mass used was less than 1.0 mg for all runs. From Figure 7, the endothermic peak at 242 °C for AP is due to a crystallographic transition of AP from orthorhombic to cubic. The second peak is exothermic, which corresponds to the low-temperature decomposition (LTD) process. The third peak is assigned to the high-temperature decomposition (HTD) process, which can be either exothermic or endothermic, depending on the competition between sublimation and thermal decomposition.[31,32] The exothermic peak of the LTD process is at about 288 °C at a heating rate of 10 °C min^{-1} (Figure 7), corresponding to the decomposition of AP with a heat of 1.47 kJ g^{-1},whereas the HTD process is an endothermic process in the temperature range 337–397 °C with a heat of 0.68 kJ g^{-1} (Figure 7).

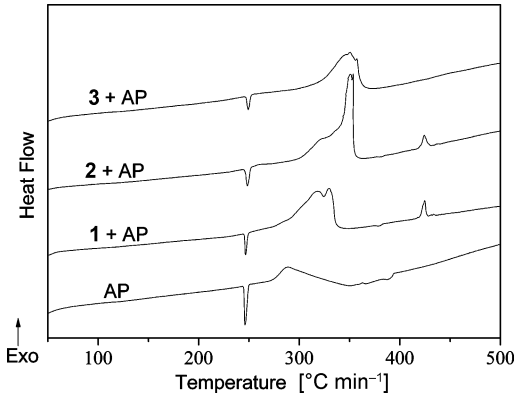

Figure 7. DSC curves for AP, **1** + AP, **2** + AP, and **3** + AP.

As shown in Figure 7, all compounds prepared in this work have no significant impact on the phase transition of AP. The LTD and HTD processes of AP become one exothermic process in the temperature range from 250 to 380 °C after adding (bta)Pb^{II} compounds. The exothermic band has two peaks after adding **1**. In the presence of **2**, the sharp decomposition peak indicates a rapid process of decomposition. As is the case in **1**, the decomposition peak for AP with **3** is wide and broad. The decomposition heats increased dramatically after adding (bta)Pb^{II} compounds (6.34, 5.69, and 6.23 kJ g^{-1} for **1**, **2**, and **3**, respectively), as shown in Table 1.

Table 1. Kinetic parameters of thermal decomposition for AP and AP with additives (T_p and ΔH were given at the heating rate of 10 °C min^{-1}).

	T_p [°C]	ΔH [kJ g^{-1}]	E_a [kJ mol^{-1}]	ln[A/s]	r
AP	288	1.47	94.48	6.72	0.992
1 +AP	341	6.34	138.74	9.93	0.995
2 +AP	354	5.69	330.12	25.9	0.995
3 +AP	362	6.23	130.71	8.82	0.996

It can be inferred that the inclusion of the (bta)Pb^{II} compounds improve the thermal decomposition of AP. As shown in Figure S2–S5, compounds **1**–**3** decompose in the range 250–380 °C,[10] whereas the bta ligand decomposes in the temperature range 200–320 °C.[9] Obviously, the release of bta from compounds **1**–**3** enhances the decomposition heat and serves catalytic effect towards the decomposition of AP.[33] Furthermore, the formation of metal lead at the molecular level on the propellant surface when the compounds decompose may contribute to the catalytic effect.[22,33]

It is known that the decomposition temperature is related to the heating rate (as shown in the Supporting Information). The relationship between decomposition temperature and heating rate can be described by the Kissinger correlation [Equation (1)].

$$\ln\frac{\beta}{T_p^2} = \ln\frac{AR}{E_a} - \frac{E_a}{RT_p} \quad (1)$$

where E_a is the apparent activation energy, β is the heating rate, R is the gas constant, T_p is the peak temperature, A is the pre-exponential factor. According to this equation, the value of activation E_a can be obtained by Kissinger's method at four different heating rates (see Figures S6–S9 for differential scanning calorimetry curves). For AP, the activation energy is calculated to be 94.48 kJ mol^{-1}. As shown in Table 1, in the presence of additives, the activation energies are changed to be 138.74, 330.12, and 130.71 kJ mol^{-1} with additives **1**, **2**, and **3**, respectively. Furthermore, the increase in activation energy and the corresponding increase in the A value are due to the kinetic compensation effect as reported.[34] Because the kinetic compensation effect occurs widely,[34] the ratio of E_a/ln(A) could be used to describe the reactivity.[35] Usually, a larger ratio means greater stability of the reactant. For compounds prepared, the ratios of E_a/ln(A) are 14.1, 14.0, 12.7, and 14.8 for pure AP, AP with **1**, AP with **2**, and AP with **3**, respectively. Obviously, **2** shows a better catalytic activity toward AP decomposition than **1** and **3**, which is consistent with the sharp exothermic peak of the DSC curves.

Photoluminescent Properties

The solid-state luminescence properties of compounds **1**–**3** as well as the H_2bta ligand were investigated at room temperature. The excitation wavelengths of the three compounds and H_2bta were set at 280 nm. The H_2bta ligand exhibits a strong fluorescence emission peak at λ_{max} = 395 nm, as shown in Figure 8a. Compounds **1**–**3**, as depicted Figure 8b, have two similar fluorescent emission bands: one is centered at 395 nm and the other is at 453 nm, which the free H_2bta ligand does not have. The similarity of emissions bands of **1**–**3** and free ligand at 395 nm is in agreement with the explanation that the nature of organic ligand would play a critical role in the photoluminescence mechanism of compounds. The luminescence of compounds **1**–**3** may be assigned to intraligand (IL) phosphorescent emission, whereas the presence of a heavy metal lead(II) ion facilitates intersystem crossing to successfully compete transitions in the triplet state with radiationless deactivations.[36] In addition, ligand-to-metal charge transfer (LMCT) may be partly attributed to the emission band at 453 nm. Therefore, the emission may be ascribed to the cooperative effects of intraligand emission and ligand-to-metal charge transfer (LMCT).[7]

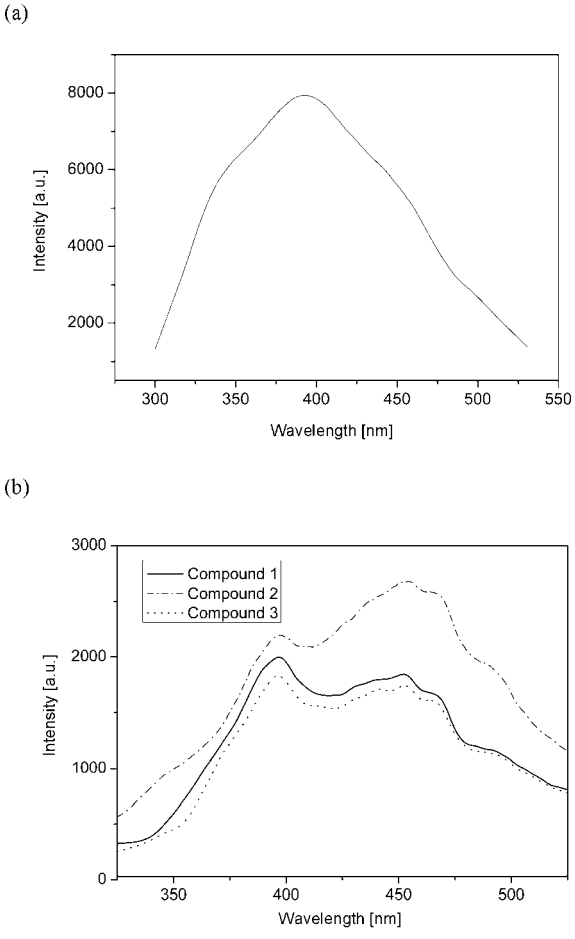

Figure 8. Emission spectra of (a) free ligand H_2bta, (b) compounds **1**, **2** and **3** in the solid state at ambient temperature (λ_{ex} = 280 nm).

Experimental Section

Caution: *H_2bta in its dehydrated form shows increased friction and impact sensitivity; (bta)lead compounds are energetic materials. Appropriate safety precautions should be taken.*

General Remarks: All reagents were purchased commercially and used without further purification. H_2bta·H_2O was synthesized according to ref.[10] Elemental analyses were carried out with an Elementar Vario EL III analyzer. IR spectra were recorded with a Tensor 27 spectrometer (Bruker Optics, Ettlingen, Germany). Fluorescent spectra were measured at room temperature with an Edinburgh FL-FS90 TCSPC system. ^{1}H NMR spectra were recorded with a Varian INOVA 400 instrument near 25 °C. Chemical shifts are reported in ppm relative to TMS. Thermogravimetric measurements were performed with a Netzsch STA449C apparatus under a nitrogen atmosphere with a heating rate of 10 °C min^{-1} from 30 to 900 °C. DSC experiments were performed with the thermal analyzer of Perkin–Elmer Pyris 6 DSC (calibrated by standard pure Indium and Zinc) with a heating rate of 5, 10, 15, 20 °C min^{-1} from 30 to 500 °C.

$[Pb(bta)(H_2O)_2]_n$ (1): A solution of $Pb(NO_3)_2$ (2 mmol) in H_2O (15 mL) was added to a pH ≈ 7 (adjusted by aqueous NaOH) solution of H_2bta·H_2O (2 mmol) in H_2O (30 mL), and a white precipitate appeared. After filtering, colorless single crystals were obtained from the mixture solution, which was allowed to evaporate at room temperature for 2 weeks. Yield: 0.0244 g (31% based on Pb). $C_2H_5N_9O_2Pb$ (394.32): calcd. C 6.09, H 1.28, N 31.97; found C 6.66, H 0.98, N 32.03. IR (KBr): $\tilde{\nu}$ = 3363 (m), 3343 (s), 3019 (s), 2882 (s), 2610 (m), 1612 (vs), 1517 (vs), 1491 (vs), 1437 (vs), 1422 (vs), 1307 (vs), 1243 (m), 1157 (w), 1108 (m), 1061 (m), 1010 (s), 798 (s), 763 (vs), 642 (m), 625 (m), 406 (m) cm^{-1}. ^{1}H NMR (400 MHz, [D$_6$]DMSO): δ = 3.34 (s, H_2O), 10.38 (s, NH) ppm.

$Pb_2(bta)_2(bpy)_2$ (2): A solution H_2bta·H_2O (2 mmol) with pH ≈ 7 (adjusted by NaOH) in H_2O (15 mL) containing was mixed with a solution of 2,2′-bipyridine (bpy; 2 mmol) in ethanol (15 mL). A solution of $Pb(NO_3)_2$ (2 mmol) in H_2O (15 mL) was added to the 30-mL mixture, and a precipitate appeared. After filtering, colorless single crystals were obtained from the mixture solution, which was allowed to evaporate at room temperature for 2 weeks. Yield: 0.0262 g (25% based on Pb). $C_{12}H_9N_{11}Pb$ (514.48): calcd. C 28.02, H 1.76, N 29.95; found C 28.20, H 1.51, N 29.91. IR (KBr): $\tilde{\nu}$ = 3270 (s), 3162 (s), 3078 (s), 1617 (vs), 1539 (s), 1499 (vs), 1452 (s), 1312 (m), 1244 (m), 1135 (m), 1076 (m), 1015 (m), 850 (s), 796 (m), 735 (m), 704 (m), 416 (w) cm^{-1}. ^{1}H NMR (400 MHz, [D$_6$]DMSO): δ = 7.46 (t, 2 H), 7.96 (t, 2 H), 8.40 (d, 2 H), 8.70 (d, 2 H), 10.38 (s, NH) ppm.

$[Pb_2(bta)_2(phen)_2]\cdot 2H_2O$ (3): A mixture of $Pb(NO_3)_2$ (0.2 mmol), 1,10-phenanthroline (0.2 mmol), and H_2bta·H_2O (0.2 mmol) in H_2O (7 mL) was sealed in a 10-mL Teflon-lined stainless autoclave and heated at 130 °C under autogenous pressure for 3 d and then cooled to room temperature; orange block crystals were obtained. Yield: 0.0236 g (22% based on Pb). $C_{14}H_9N_{11}Pb$ (538.50): calcd. C 30.22, H 1.99, N 27.69; found C 30.52, H 1.64, N 27.77. IR (KBr): $\tilde{\nu}$ = 3385 (m), 3358 (m), 3141 (m), 3024 (s), 2829 (s), 2802 (s), 2625 (w), 1623 (vs), 1507 (vs), 1422 (vs), 1385 (s), 1312 (s), 1145 (w), 1101 (m), 1032 (w), 1007 (w), 893 (s), 842 (s), 722 (vs), 638 (m) cm^{-1}. ^{1}H NMR (400 MHz, [D$_6$]DMSO): δ = 3.34 (s, H_2O), 7.66 (t, 2 H), 7.82 (s, 2 H), 8.27 (d, 2 H), 9.21 (d, 2 H), 10.38 (s, NH) ppm.

X-ray Crystallography: All single-crystal X-ray experiments were performed with a Bruker Smart Apex CCD diffractometer equipped with graphite monochromated Mo-K_α radiation (λ = 0.71073 Å) using ω and ϕ scan mode. The single-crystal structures

of compounds were both solved by direct methods and refined with full-matrix least-squares refinements based on F^2 using SHELXS-97 and SHELXL-97. All non-hydrogen atoms were refined anisotropically. Selected bond lengths and angles are tabulated in Table S1 and selected hydrogen-bonding geometries for **1**, **2**, and **3** are listed in Table S2.

Compound 1: $C_2H_5N_9O_2Pb$, M = 394.35, monoclinic, space group $P2_1/n$ (No. 14), a = 6.6299(12) Å, b = 12.023(2) Å, c = 12.023(2) Å, β = 104.858(2) °, V = 814.9(2) Å^3, Z = 4, T = 293(2) K, F(000) = 712, $D_{calcd.}$ = 3.214 g cm^{-3}, R_1 = 0.0270, wR_2 = 0.0657 and GOF = 1.02 for 127 parameters, 1424 reflections with $|F_o| \geq 4\sigma(F_o)$.

Compound 2: $C_{24}H_{18}N_{22}Pb_2$, M = 1029.00, triclinic, space group $P\bar{1}$ (No. 2), a = 6.8790(11) Å, b = 9.6869(15) Å, c = 10.6843(17) Å, α = 94.735(2)°, β = 92.880(2)°, γ = 96.419(2)°, V = 703.81(19) Å^3, Z = 1, T = 293(2) K, F(000) = 480, $D_{calcd.}$ = 2.428 g cm^{-3}, R_1 = 0.0525, wR_2 = 0.1590 and GOF = 1.17 for 217 parameters, 2430 reflections with $|F_o| \geq 4\sigma(F_o)$.

Compound 3: $C_{28}H_{18}N_{22}Pb_2H_4O_2$, M = 1113.08, monoclinic, space group $C2/c$ (No. 15), a = 9.406(3) Å, b = 22.860(7) Å, c = 15.300(5) Å, β = 105.887(5)°, V = 3164.4(17) Å^3, Z = 4, T = 293(2) K, F(000) = 2096, $D_{calcd.}$ = 2.336 g cm^{-3}, R_1 = 0.0567, wR_2 = 0.1675 and GOF = 1.04 for 244 parameters, 2777 reflections with $|F_o| \geq 4\sigma(F_o)$.

CCDC-650737 (for **1**), -721842 (for **2**), and -721843 (for **3**) contain the supplementary crystallographic data for this paper. These data can be obtained free of charge from The Cambridge Crystallographic Data Centre via www.ccdc.cam.ac.uk/data_request/cif.

Supporting Information (see footnote on the first page of this article): Selected bond lengths, angles, and hydrogen-bonding interactions for **1**–**3**; TG curves and DSC curves for **1**–**3**; 3D supramolecular frame for **3**.

Acknowledgments

We are grateful for the financial support of the National Science Foundation of China (Nos. 20771089, 20873100) and the Natural Science Foundation of Shaanxi Province (Nos. 2007B02, SJ08B09).

[1] G. Singh, S. Prem Felix, *J. Hazard. Mater.* **2002**, *90*, 1–17.
[2] G. Singh, R. Prajapati, R. Frohlich, *J. Hazard. Mater.* **2005**, *118*, 75–78.
[3] N. Liu, Q. Yue, Y. Q. Wang, A. L. Cheng, E. Q. Gao, *Dalton Trans.* **2008**, 4621–4629.
[4] Y. F. Guan, D. Y. Wang, W. Dong, *Acta Crystallogr., Sect. E* **2007**, *63*, m3150–m3150.
[5] T. Jiang, X. M. Zhang, *Cryst. Growth Des.* **2008**, *8*, 3077–3083.
[6] E. Q. Gao, N. Liu, A. L. Cheng, S. Gao, *Chem. Commun.* **2007**, 2470–2472.
[7] L. L. Zheng, H. X. Li, J. D. Leng, J. Wang, M. L. Tong, *Eur. J. Inorg. Chem.* **2008**, 213–217.
[8] Y. B. Lu, M. S. Wang, W. W. Zhou, G. Xu, G. C. Guo, J. S. Huang, *Inorg. Chem.* **2008**, *47*, 8935–8942.
[9] D. E. G. Jones, K. Armstrong, T. Parekunnel, Q. S. M. Kwok, *J. Therm. Anal. Calorim.* **2006**, *86*, 641–649.
[10] M. Friedrich, J. C. Gálvez-Ruiz, T. M. Klapötke, P. Mayer, B. Weber, J. J. Weigand, *Inorg. Chem.* **2005**, *44*, 8044–8052.
[11] R. P. Singh, R. D. Verma, D. T. Meshri, J. M. Shreeve, *Angew. Chem. Int. Ed.* **2006**, *45*, 3584–3601.
[12] L. J. Chen, L. P. Li, G. S. Li, *J. Alloys Compd.* **2008**, *464*, 532–536.
[13] P. Cui, F. S. Li, J. Zhou, W. Jiang, *Propellants Explos. Pyrotech.* **2006**, *31*, 452–455.
[14] T. Liu, L. S. Wang, P. Yang, B. Y. Hu, *Mater. Lett.* **2008**, *62*, 4056–4058.
[15] A. A. Said, R. Al-Qasmi, *Thermochim. Acta* **1996**, *275*, 83–91.
[16] X. F. Sun, X. Q. Qiu, L. P. Li, G. S. Li, *Inorg. Chem.* **2008**, *47*, 4146–4152.
[17] D. V. Survase, M. Gupta, S. N. Asthana, *Prog. Cryst. Growth Charact. Mater.* **2002**, *45*, 161–165.
[18] Y. P. Wang, J. W. Zhu, X. J. Yang, L. D. Lu, X. Wang, *Thermochim. Acta* **2005**, *437*, 106–109.
[19] H. Xu, X. B. Wang, L. Z. Zhang, *Powder Technol.* **2008**, *185*, 176–180.
[20] L. J. Chen, G. S. Li, L. P. Li, *J. Therm. Anal. Calorim.* **2008**, *91*, 581–587.
[21] G. Singh, S. P. Felix, *Combust. Flame* **2003**, *132*, 422–432.
[22] P. B. Kulkarni, T. S. Reddy, J. K. Nair, A. N. Nazare, M. B. Talawar, T. Mukundan, S. N. Asthana, *J. Hazard. Mater.* **2005**, *123*, 54–60.
[23] S. M. Pundlik, R. S. Palaiah, J. K. Nair, T. Mukundan, S. N. Singh, H. Singh, *J. Energ. Mater.* **2001**, *19*, 339–347.
[24] R. L. Davidovich, V. Stavila, D. V. Marinin, E. I. Voit, K. H. Whitmirec, *Coord. Chem. Rev.* **2008**, *253*, 1316–1352.
[25] J. Yang, G.-D. Li, J.-J. Cao, Q. Yue, G.-H. Li, J.-Sh. Chen, *Chem. Eur. J.* **2007**, *13*, 3248–3261.
[26] A. M. P. Peedikakkal, J. J. Vittal, *Cryst. Growth Des.* **2008**, *8*, 375–377.
[27] S. N. Semenov, A. Y. Rogachev, S. V. Eliseeva, Y. A. Belousov, A. A. Drozdov, S. I. Troyanov, *Polyhedron* **2007**, *26*, 4899–4907.
[28] M. C. Etter, *Acc. Chem. Res.* **1990**, *23*, 120–126.
[29] J.-M. Lin, B.-S. Huang, Y.-F. Guan, Z.-Q. Liu, D.-Y. Wang, W. Dong, *CrystEngComm* **2009**, *11*, 329–336.
[30] H. Zhao, Z. R. Qu, H. Y. Ye, R. G. Xiong, *Chem. Soc. Rev.* **2008**, *37*, 84–100.
[31] A. J. Lang, S. Vyazovkin, *Combust. Flame* **2006**, *145*, 779–790.
[32] S. Vyazovkin, C. A. Wight, *Chem. Mater.* **1999**, *11*, 3386–3393.
[33] M. B. Talawar, C. N. Divekar, P. S. Makashir, S. N. Asthana, *J. Propul. Power* **2005**, *21*, 186–189.
[34] T. B. Brill, P. E. Gongwer, G. K. Williams, *J. Phys. Chem.* **1994**, *98*, 12242–12247.
[35] B. Andričić, T. Kovačić, I. Klarić, *Polym. Degrad. Stab.* **2003**, *79*, 265–270.
[36] Q. Y. Liu, X. Li, *Eur. J. Inorg. Chem.* **2006**, 1620–1628.

Received: April 13, 2009
Published Online: July 9, 2009

